International Journal of Heat and Mass Transfer 51 (2008) 5238–5246

Contents lists available at ScienceDirect

International Journal of Heat and Mass Transfer

journal homepage: www.elsevier.com/locate/ijhmt

A transient three-dimensional inverse geometry problem in estimating the space and time-dependent irregular boundary shapes

Cheng-Hung Huang *, Meng-Ting Chaing

Department of Systems and Naval Mechatronic Engineering, National Cheng Kung University, No. 1, University Road, Tainan, Taiwan, ROC

ARTICLE INFO

Article history:
Received 4 September 2007
Received in revised form 17 March 2008
Available online 28 May 2008

ABSTRACT

A transient three-dimensional shape identification problem (inverse geometry problem) to determine the unknown irregular and moving boundary configurations by utilizing the steepest descend method (SDM) and a general purpose commercial code CFD-RC is successfully developed and examined in this study based on the simulated measured temperature distributions on the bottom surface by infrared thermography. The advantage of calling CFD-RC as a subroutine in the present inverse calculation lies in that its auto-mesh function enables the handling of this moving boundary problem. Results obtained by using the technique of SDM to solve the inverse geometry problem are justified based on the numerical experiments. Two test cases are performed to test the validity of the present algorithm by using different types of boundary shapes, initial guesses and measurement errors. Results show that reliable estimations on the unknown space and time-dependent boundary geometry can be obtained when the measurement errors are considered.

1. Introduction

The direct heat conduction problems are concerned with the determination of temperature at interior points of a region when the initial and boundary conditions, thermophysical properties and heat generation are specified. In contrast, the inverse heat conduction problem involves the determination of the unknown physical conditions from the knowledge of temperature measurements taken on or within the domain where the geometry of the physical problem under consideration is known. For instance, Huang and Chen [1] used the conjugate gradient method (CGM) in estimating surface heat fluxes for a three-dimensional inverse heat convection problem. Huang and Huang [2] used the CGM in an inverse biotechnology problem to estimate the optical diffusion and absorption coefficients of tissue. Huang and Lo [3] applied the SDM in a three-dimensional inverse problem in predicting the heat fluxes distribution of the cutting tools. However, when the geometry of the problems is subjected to change and unknown, i.e. the boundary is moving, the technique of inverse geometry problem (IGP) should be used to estimate the space and time-dependent boundary configurations.

The application of inverse geometry problem, such as thermal imaging, has become another area of active inverse problem research recently and many researchers have devoted to infrared scanner and their applications to nondestructive evaluation (NDE) [4] and shape identifications [5] problems. Dems and Mroz [6] investigated the sensitivity analysis for static and quasi-static problems with respect to size and shape design variables. The approaches taken to solve these problems are based on either steady or unsteady-state response of a body subjected to thermal sources.

For the transient inverse geometry problem, due to its inherent nature of moving boundary, it requires a complete regeneration of the mesh as the geometry evolves. Moreover, the continuous evolution of the geometry itself poses certain difficulties in arriving at analytical or numerical solutions. Therefore, an efficient technique must be used to calculate the problems with irregular and moving boundary geometry, especially in the 3D applications.

The inverse geometry problems, including the cavity or shape estimation, have been solved by a variety of numerical methods [7–9]. Huang and his co-workers have utilized the gradient-based method (SDM and CGM) and boundary element technique to the inverse geometry problems and have published a series of relevant papers. Huang and Chao [10] were the first to derive the formulations for determining the unknown irregular boundary configurations for a 2D steady-state shape identification problem with the CGM. Huang and Tsai [11] have extended the algorithm to a 2D transient shape identification problem in finding the unknown irregular boundary configurations from boundary measurements. Huang et al. [12] have developed a modified model for two-dimensional multiple cavities estimations where the search directions are not confined. Huang and Chen [13] have extended the similar algorithm to a multiple region domain in estimating the time and space-dependent outer boundary configurations. Recently

* Corresponding author. Tel.: +886 6 2747018; fax: +886 6 2747019.
E-mail address: chhuang@mail.ncku.edu.tw (C.-H. Huang).

0017-9310/$ - see front matter © 2008 Elsevier Ltd. All rights reserved.
doi:10.1016/j.ijheatmasstransfer.2008.03.019

Nomenclature

C_p	heat capacity per unit volume
$f(x,y,t)$	unknown boundary configurations
J	functional defined by Eq. (2)
J'	gradient of functional defined by Eq. (14)
k	thermal conductivity
P	direction of descent defined by Eq. (4)
q	heat flux density
$T(x,y,z,t)$	estimated temperature
T_0	boundary temperature on S_{top}
$\Delta T(x,y,z,t)$	sensitivity function defined by Eq. (5)
$Y(S_{bottom},t)$	measured temperatures

Greek symbols

β	search step size
ρ	density
Ω	computational domain
$\lambda(x,y,z,t)$	Lagrange multiplier defined by Eq. (11)
$\delta(\cdot)$	Dirac delta function
ω	random number
ε	convergence criterion
σ	standard deviation of the measurement errors

Superscript

n	iteration index

Huang and Shih [14] applied the technique to a shape identification problem in estimating simultaneously two interfacial configurations in a multiple region domain.

It should be noted that the above references are all 2D inverse geometry problems; the steady 3D inverse geometry problems are still very limited in the literatures. Recently, Divo et al. [15] used the genetic algorithm and a singular superposition technique to detect the unknown sphere cavity in a 3D inverse geometry problem. It should be noted that the transient 3D inverse geometry problem with SDM has never been examined in the opening literatures.

The commercial code CFD-RC [16] is available for solving fluid dynamic and heat transfer problems with the feature of auto-meshing. If one can link the CFD-RC with an inverse algorithm, a generalized transient 3D inverse geometry problem can thus be established. The objective of the present study is to extend the previous studies on the inverse geometry problems by the authors [11–14] and to utilize the CFD-RC code as the subroutine to solve the transient 3D inverse geometry problem by the SDM. The application of this technique can be used in estimating the unknown interface of the solid and liquid phases for the phase change problems.

A sequence of forward transient heat conduction problems is solved by CFD-RC in an effort to update the boundary shape by minimizing a residual measuring the difference between estimated and measured temperatures under the present algorithm.

The SDM derives from the perturbation principles [17] and transforms the inverse geometry problem to the solution of three problems, namely, the direct, sensitivity and the adjoint problem. Those three problems can be solved by CFD-RC and the calculated results are then utilized in the SDM for shape identifications.

2. The direct problem

To show the methodology for developing expressions for use in determining unknown space and time-dependent boundary geometry in a three-dimensional homogeneous medium, the following three-dimensional unsteady-state inverse heat conduction problem is examined. Initially, the domain Ω has the uniform temperature T_i. When time $t > 0$, the boundary conditions on four side surfaces S_1, S_2, S_3 and S_4 are all assumed insulated, on the bottom surface S_{bottom}, a constant heat flux q is taken away from the boundary by cooling while the boundary condition on the top surface S_{top}, $z = f(x,y,t)$, maintains at an uniform temperature T_0. Fig. 1 shows the geometry and the coordinates for the transient three-dimensional physical problem considered here. The mathematical

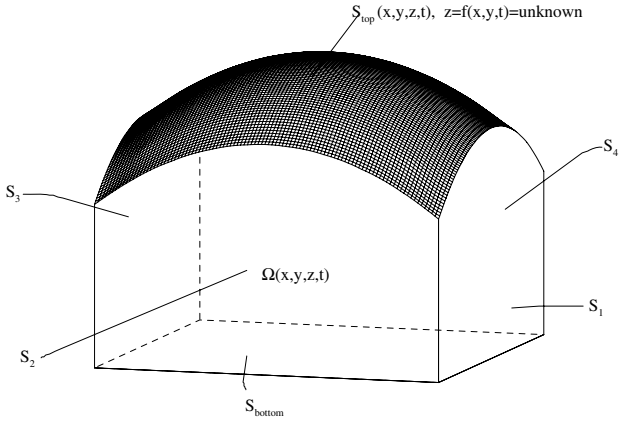

Fig. 1. Geometry and coordinates.

formulation of this unsteady-state heat conduction problem in dimensional form is given by

$$k\left[\frac{\partial^2 T}{\partial x^2}+\frac{\partial^2 T}{\partial y^2}+\frac{\partial^2 T}{\partial z^2}\right]=\rho C_p\frac{\partial T}{\partial t} \quad \text{in } \Omega,\ t>0 \tag{1a}$$

$$\frac{\partial T}{\partial x}=0 \quad \text{on } S_1,\ t>0 \tag{1b}$$

$$\frac{\partial T}{\partial x}=0 \quad \text{on } S_2,\ t>0 \tag{1c}$$

$$\frac{\partial T}{\partial y}=0 \quad \text{on } S_3,\ t>0 \tag{1d}$$

$$\frac{\partial T}{\partial y}=0 \quad \text{on } S_4,\ t>0 \tag{1e}$$

$$k\frac{\partial T}{\partial z}=q(S_{bottom},t) \quad \text{on } S_{bottom},\ t>0 \tag{1f}$$

$$T=T_0 \quad \text{on } S_{top},\ z=f(x,y,t),\ t>0 \tag{1g}$$

$$T=T_i \quad \text{at } t=0 \tag{1h}$$

where k, C_p and ρ denote the thermal conductivity, heat capacity and density, respectively, and q is the heat flux. The above problem is solved by the commercial package CFD-RC [16] for it has the ability to perform the auto-mesh function and to solve the moving boundary problems.

The direct problem considered here is concerned with the determination of the body temperatures when the space and time-dependent boundary geometry $f(x,y,t)$, initial condition and boundary conditions at all boundaries are known.

3. The inverse geometry problem

For the transient three-dimensional inverse geometry problem considered here, the boundary space and time-dependent geometry $f(x,y,t)$ is regarded as being unknown, but everything else in Eq. (1) is known. In addition, the simulated temperature readings taken by infrared scanner on the bottom surface S_{bottom} with time are considered available.

Referring to Fig. 1, let the temperature reading taken by the simulated infrared scanner on the bottom surface S_{bottom} be denoted by $\mathbf{Y}(S_{\text{bottom}},t) \equiv Y(x_m,y_m,t) \equiv Y_m(S_{\text{bottom}},t)$, $m = 1$ to M, where M represents the number of measured temperature extracting points and t denotes time. It is noted that the measured temperature $Y_m(S_{\text{bottom}},t)$ should contain measurement errors. The present shape identification problem can be stated as follows: by utilizing the above mentioned measured temperature data $Y_m(S_{\text{bottom}},t)$, estimate the unknown space and time-dependent geometry on the top surface, $z = f(x,y,t)$.

The solution of this inverse geometry problem is to be obtained in such a way that the following functional is minimized:

$$J[f(x,y,t)] = \int_{t=0}^{t_f} \sum_{m=1}^{M} [T_m(S_{\text{bottom}},t) - Y_m(S_{\text{bottom}},t)]^2 \mathrm{d}t = \int_{t=0}^{t_f} \int_{S_{\text{bottom}}} (T-Y)^2 \delta(x-x_m)\delta(y-y_m)\mathrm{d}S_{\text{bottom}}\,\mathrm{d}t \tag{2}$$

where $\delta(x-x_m)$ and $\delta(y-y_m)$ are the Dirac delta functions and T_m are the estimated or computed temperatures on the measured positions (x_m,y_m) on S_{bottom} with time t. These quantities are determined from the solution of the direct problem given previously by using estimated boundary geometry for the exact $f(x,y,t)$.

4. Steepest descent method for minimization

The steepest descent method itself may not ensure the global minimum; however, if the objective function is properly defined and makes it in a quadratic form, like the definition in Eq. (2), the global minimum for this objective function is guarantied.

The following iterative process based on the SDM [17] is now used for the estimation of unknown space and time-dependent boundary geometry $f(x,y,t)$ by minimizing the functional $J[f(x,y,t)]$

$$f^{n+1}(x,y,t) = f^n(x,y,t) - \beta^n P^n(x,y,t) \quad \text{for } n = 0,1,2,\ldots \tag{3}$$

where β^n is the search step size in going from iteration n to iteration $n+1$, and $P^n(x,y,t)$ is the direction of descent (i.e. search direction) given by

$$P^n(x,y,t) = J'^n(x,y,t) \tag{4}$$

which is equal to the gradient direction $J'^n(x,y,t)$ at iteration n.

To perform the iterations according to Eq. (3), a search step size β^n and the gradient of the functional $J'^n(x,y,t)$ need be computed. In order to develop expressions for the determination of these two quantities, a sensitivity problem and an adjoint problem are constructed as described below.

5. Sensitivity problem and search step size

The sensitivity problem is obtained from the original direct problem defined by Eq. (1) in the following manner: It is assumed that when $z = f(x,y,t)$ undergoes a variation Δz (or $\Delta f(x,y,t)$) in z-direction only with both x and y fixed, $T(x,y,z,t)$ is perturbed by $\Delta T(x,y,z,t)$. Replacing in the direct problem f by $f+\Delta f$ and T by $T+\Delta T$, subtracting the direct problem from the resulting expressions and neglecting the second-order terms, the following sensitivity problem for determining the sensitivity function ΔT is obtained:

$$k\left[\frac{\partial^2\Delta T}{\partial x^2} + \frac{\partial^2\Delta T}{\partial y^2} + \frac{\partial^2\Delta T}{\partial z^2}\right] = \rho C_p \frac{\partial \Delta T}{\partial t} \quad \text{in } \Omega,\ t>0 \tag{5a}$$

$$\frac{\partial \Delta T}{\partial x} = 0 \quad \text{on } S_1,\ t>0 \tag{5b}$$

$$\frac{\partial \Delta T}{\partial x} = 0 \quad \text{on } S_2,\ t>0 \tag{5c}$$

$$\frac{\partial \Delta T}{\partial y} = 0 \quad \text{on } S_3,\ t>0 \tag{5d}$$

$$\frac{\partial \Delta T}{\partial y} = 0 \quad \text{on } S_4,\ t>0 \tag{5e}$$

$$\frac{\partial \Delta T}{\partial z} = 0 \quad \text{on } S_{\text{bottom}},\ t>0 \tag{5f}$$

$$\Delta T = \Delta f \frac{\partial T}{\partial z} \quad \text{on } S_{\text{top}},\quad z = f(x,y,t),\ t>0 \tag{5g}$$

$$\Delta T = 0 \quad \text{at } t = 0 \tag{5h}$$

The commercial package CFD-RC is utilized to solve the above sensitivity problem. The functional $J(f^{n+1})$ for iteration $n+1$ is obtained by rewriting Eq. (2) as

$$J(f^{n+1}) = \int_{t=0}^{t_f} \int_{S_{\text{bottom}}} [T(S_{\text{bottom}},t;f^n - \beta^n P^n) - Y]^2 \times \delta(x-x_m)\delta(y-y_m)\mathrm{d}S_{\text{bottom}}\,\mathrm{d}t \tag{6}$$

where $f^{n+1}(x,y,t)$ has been replaced by the expression given by Eq. (3). If temperature $T(S_{\text{bottom}},t;f^n - \beta^n P^n)$ is linearized by a Taylor's expansion, Eq. (6) becomes

$$J(f^{n+1}) = \int_{t=0}^{t_f} \int_{S_{\text{bottom}}} [T(S_{\text{bottom}},t;f^n) - \beta^n \Delta T(S_{\text{bottom}},t;P^n) - Y]^2 \times \delta(x-x_m)\delta(y-y_m)\mathrm{d}S_{\text{bottom}}\,\mathrm{d}t \tag{7}$$

where $T(S_{\text{bottom}},t;f^n)$ is the solution of the direct problem by using the estimated $f^n(x,y,t)$ for exact $f(x,y,t)$ on the top surface S_{top}. The sensitivity functions $\Delta T(S_{\text{bottom}},t;P^n)$ are taken as the solutions of problem (5) on S_{bottom} with time t by letting $\Delta f = P^n$.

The search step size β^n can be determined by minimizing the functional given by Eq. (7) with respect to β^n. The following expression results:

$$\beta^n = \frac{\int_{t=0}^{t_f}\int_{S_{\text{bottom}}} (T-Y)\Delta T\delta(x-x_m)\delta(y-y_m)\mathrm{d}S_{\text{bottom}}\,\mathrm{d}t}{\int_{t=0}^{t_f}\int_{S_{\text{bottom}}} (\Delta T)^2\delta(x-x_m)\delta(y-y_m)\mathrm{d}S_{\text{bottom}}\,\mathrm{d}t} \tag{8}$$

6. Adjoint problem and gradient equation

To obtain the adjoint problem, Eq. (1a) is multiplied by a Lagrange multiplier (or adjoint function) $\lambda(x,y,z,t)$ and the resulting expression is integrated over the correspondent space and time domains. The result is then added to the right hand side of Eq. (2) to yield the following expression for the functional $J[f(x,y,t)]$:

$$J[f(x,y,t)] = \int_{t=0}^{t_f} \int_{S_{\text{bottom}}} (T-Y)^2\delta(x-x_m)\delta(y-y_m)\mathrm{d}S_{\text{bottom}}\,\mathrm{d}t + \int_{t=0}^{t_f}\int_{x=0}^{L}\int_{y=0}^{L} \times \int_{z=0}^{f(x,y,t)} \lambda(x,y,z,t)\left\{\frac{\partial^2 T}{\partial x^2} + \frac{\partial^2 T}{\partial y^2} + \frac{\partial^2 T}{\partial z^2}\right\}\mathrm{d}z\,\mathrm{d}y\,\mathrm{d}x\,\mathrm{d}t \tag{9}$$

The variation ΔJ is obtained by perturbing f by Δf and T by ΔT in Eq. (9), subtracting the original Eq. (9) from the resulting expression and neglecting the second-order terms. It thus finds

$$\Delta J[f(x,y,t)] = \int_{t=0}^{t_f}\int_{S_{\text{bottom}}} 2[T-Y]\Delta T\delta(x-x_m)\delta(y-y_m)\mathrm{d}S_{\text{bottom}}\,\mathrm{d}t + \int_{t=0}^{t_f}\int_{x=0}^{L}\int_{y=0}^{L}\times\int_{z=0}^{f(x,y,t)}\lambda(x,y,z,t)\left\{\frac{\partial^2\Delta T}{\partial x^2}+\frac{\partial^2\Delta T}{\partial y^2}+\frac{\partial^2\Delta T}{\partial z^2}\right\}\mathrm{d}z\,\mathrm{d}y\,\mathrm{d}x\,\mathrm{d}t \tag{10}$$

where $\delta(x-x_m)$ and $\delta(y-y_m)$ are the Dirac delta function and (x_m,y_m), $n=1$ to M, refer to the temperature extracting points at time t. In Eq. (10), the integral term containing $\lambda(x,y,z,t)$ is integrated by parts; the boundary conditions of the sensitivity problem given by Eqs. (5b)–(5g) are utilized and then ΔJ is allowed to go to zero. The vanishing of the integrands containing ΔT leads to the following adjoint problem for the determination of $\lambda(x,y,z,t)$:

$$k\left[\frac{\partial^2\lambda}{\partial x^2}+\frac{\partial^2\lambda}{\partial y^2}+\frac{\partial^2\lambda}{\partial z^2}\right]+\rho C_p\frac{\partial\lambda}{\partial t}=0 \quad \text{in } \Omega,\ t>0 \tag{11a}$$

$$\frac{\partial\lambda}{\partial x}=0 \quad \text{on } S_1,\ t>0 \tag{11b}$$

$$\frac{\partial\lambda}{\partial x}=0 \quad \text{on } S_2,\ t>0 \tag{11c}$$

$$\frac{\partial\lambda}{\partial y}=0 \quad \text{on } S_3,\ t>0 \tag{11d}$$

$$\frac{\partial\lambda}{\partial y}=0 \quad \text{on } S_4,\ t>0 \tag{11e}$$

$$\frac{\partial\lambda}{\partial z}=-2(T-Y)\delta(x-x_m)\delta(y-y_m) \quad \text{on } S_{\text{bottom}},\ t>0 \tag{11f}$$

$$\lambda=0 \quad \text{on } S_{\text{top}}=f(x,y,t),\ t>0 \tag{11g}$$

$$\lambda=0 \quad \text{at } t=t_f \tag{11h}$$

The adjoint problem differs from the standard initial value problems in that the final time conditions at time $t=t_f$ is specified instead of the customary initial condition. However, this adjoint problem can be transformed to an initial value problem by the transformation of the time variables as $\tau=t_f-t$. The CFD-RC can then be used to solve the above adjoint problem.

Finally, the following integral term is left:

$$\Delta J=\int_{t=0}^{t_f}\int_{S_{\text{top}}}-\left[\frac{\partial\lambda}{\partial z}\frac{\partial T}{\partial z}\right]_{z=f(x,y,t)}\Delta f(x,y,t)\mathrm{d}S_{\text{top}}\,\mathrm{d}t \tag{12}$$

From definition [17], the functional increment can be presented as

$$\Delta J=\int_{t=0}^{t_f}\int_{S_{\text{top}}}J'(x,y,t)\Delta f(x,y,t)\mathrm{d}S_{\text{top}}\,\mathrm{d}t \tag{13}$$

A comparison of Eqs. (12) and (13) leads to the following expression for the gradient of functional $J'(x,y,t)$ of the functional $J[f(x,y,t)]$:

$$J'(x,y,t)=-\frac{\partial\lambda}{\partial z}\frac{\partial T}{\partial z}\bigg|_{z=f(x,y,t)} \tag{14a}$$

It is noted that $J'(x,y,0)$ and $J'(x,y,t_f)$ are always equal to zero since $\frac{\partial\lambda(x,y,z,t_f)}{\partial z}=0$ and $\frac{\partial T(x,y,z,0)}{\partial z}=0$. If the initial values of $f(x,y,0)$ and final time values of $f(x,y,t_f)$ cannot be obtained before the shape identify calculations, the estimated values of $f(x,y,t)$ will deviate from the exact values near both initial and final time conditions. This is the case in the present study. However, if we let

$$\frac{\partial T(x,y,z,0)}{\partial z}=\frac{\partial T(x,y,z,\Delta t)}{\partial y} \tag{14b}$$

$$\frac{\partial\lambda(x,y,z,t_f)}{\partial z}=\frac{\partial\lambda(x,y,z,t_f-\Delta t)}{\partial z} \tag{14c}$$

where Δt denotes the time increment used in the numerical calculation. By applying (14b) and (14c) to the gradient equation (14a), the singularity at $t=0$ and t_f can be avoided in the present study and the reliable inverse solutions can be obtained.

7. Stopping criterion

If the problem contains no measurement errors, the traditional check condition is specified as

$$J[f^{n+1}(x,y,t)]<\varepsilon \tag{15}$$

where ε is a specified number. However, the simulated temperature readings taken by infrared scanner may contain measurement errors. Therefore, it is not expected that the functional equation (2) to be equal to zero at the final iteration step. Following the experience of the authors [11–14], the discrepancy principle is utilized as the stopping criterion, i.e. the temperature residuals may be approximated by

$$T(S_{\text{bottom}},t)-Y(S_{\text{bottom}},t)\approx\sigma \tag{16}$$

where σ is the standard deviation of the temperature measurements, which is assumed to be a constant. Substituting Eq. (16) into Eq. (2), the following expression is obtained for ε:

$$\varepsilon=\sigma^2 M t_f \tag{17}$$

The stopping criterion is given by Eq. (15) with ε determined from Eq. (17).

8. Computational procedure

The computational procedure for the solution of this transient three-dimensional inverse geometry problem using the SDM can now be summarized as follows.

Suppose $f^n(x,y,t)$ is available at iteration n:

Step 1: Solve the direct problem given by Eq. (1) for $T(x,y,z,t)$.
Step 2: Examine the stopping criterion ε for convergence.Continue if not satisfied.
Step 3: Solve the adjoint problem given by Eq. (11) for $\lambda(x,y,z,t)$.
Step 4: Compute the gradient of the functional $J'(x,y,t)$ from Eq. (14a).
Step 5: Compute the direction of descent P^n from Eq. (4).
Step 6: Set $\Delta f(x,y,t)=P^n(x,y,t)$, and solve the sensitivity problem given by Eq. (5) for $\Delta T(x,y,z,t)$.
Step 7: Compute the search step size β^n from Eq. (8).
Step 8: Compute the new estimation for $f^{n+1}(x,y,t)$ from Eq. (3) and return to step 1.

9. Results and discussion

To illustrate the validity of the SDM in identifying space and time-dependent boundary configuration $z=f(x,y,t)$ in a 3D boundary shapes identification problem based on the knowledge of the simulated temperature recordings taken by infrared scanner on the bottom surface S_{bottom} with time t, two specific examples were considered in this study where the surface geometry on S_{top}, $z=f(x,y,t)$, are assumed as two different functions, the first one is a combination of sine and cosine functions and the second one is a combination of triangular functions.

The goal of this work is to show the validity of the SDM in estimating $f(x,y,t)$ with no prior information on the functional form of the unknown quantities, which is the so-called function estimation.

In order to compare the results for situations involving random measurement errors, the normally distributed uncorrelated errors with zero mean and constant standard deviation were assumed. The simulated inexact measurement data $\mathbf{Y}$ can be expressed as

$$\mathbf{Y}=\mathbf{Y}_{\text{dir}}+\omega\sigma \tag{18}$$

where $\mathbf{Y}_{\text{dir}}$ is the solution of the direct problem with an exact $f(x,y,t)$; σ is the standard deviation of the measurement error; and

ω is a random variable that generated by subroutine DRNNOR of the IMSL [18] and will be within −2.576 to 2.576 for a 99% confidence bounds.

One of the advantages of using the SDM is that it does not require a very accurate initial guess of the unknown quantities, this can be verified in the following numerical test case 1.

In all the test cases considered here the following parameters are chosen, $k = 76.2$ W/(m K), $\rho = 7870$ kg/m^3, $C_p = 440$ J/(kg K), L_x (length in x-direction) = L_y (length in y-direction) = 0.5 m, and the spacing in numerical computations is taken as $\Delta x = \Delta y = 0.05$ m, i.e. there are 11 grid points in both x- and y-direction. In z-direction, five grids are always chosen for computations. In time domain, total time is taken as 200 s and $\Delta t = 20$ s is used in numerical calculations. Therefore, there is totally of 2420 discreted boundary shapes need to be estimated in this study.

The initial temperature $T_i = 23$ °C and boundary condition $T_0 = 127$ °C is applied on S_{top}. The measurement surface is always on S_{bottom}, i.e. on the bottom surface. Two numerical experiments in estimating $f(x,y,t)$ by the inverse analysis are now presented below.

9.1. Numerical test case 1

The unknown boundary configuration on S_{top}, $z = f(x,y,t)$, is assumed in the following form:

$$f(x,y,t) = 0.05 + 0.015 \times \left(\sin\frac{2\pi x}{0.1}\right) \times \left(\cos\frac{2\pi y}{0.1}\right) \times \left(\sin\frac{2\pi t}{200}\right) \tag{19}$$

which represents a combination of sine and cosine functions.

The inverse analysis is first performed by using $q = -50{,}000$ W/m^2 and assuming exact measurements, i.e. $\sigma = 0.0$, and using initial guess $f(x,y,t)^0 = 0.04$ m with convergent criterion $\varepsilon = 500$.

After 21 iterations, the exact and estimated functions of $f(x,y,t)$ by using the SDM at $t = 50$ s is shown in Fig. 2a and b, respectively, while the measured and estimated surface temperatures on S_{bottom} are illustrated in Fig. 3a and b, respectively. Similarly, the estimated results for boundary shapes and temperatures at $t = 150$ s are shown in Figs. 4 and 5, respectively.

The average relative errors for the exact and estimated surface configurations and for the measured and estimated temperatures are calculated ERR1 = 1.56% and ERR2 = 0.066%, respectively, where the average relative errors ERR1 and ERR2 are defined as

$$\mathrm{ERR1} = \sum_{n=1}^{N}\sum_{m=1}^{M}\sum_{i=1}^{I}\left|\frac{f(x_n,y_m,t_i) - \hat{f}(x_n,y_m,t_i)}{f(x_n,y_m,t_i)}\right| \div (N \times M \times I) \times 100\% \tag{20a}$$

$$\mathrm{ERR2} = \sum_{n=1}^{N}\sum_{m=1}^{M}\sum_{i=1}^{I}\left|\frac{T(x_n,y_m,0,t_i) - Y(x_n,y_m,0,t_i)}{Y(x_n,y_m,0,t_i)}\right| \div (N \times M \times I) \times 100\% \tag{20b}$$

here $N = 11$ and $M = 11$ represent the total discreted number of grid in x- and y-directions, respectively and $I = 20$ indicates the number of grid in t-direction, while f and $\hat{f}$ denote the exact and estimated values of surface configurations, respectively. It can be seen from the above figures and relative average errors that the present shape identification scheme obtained good estimation for $f(x,y,t)$.

Next, it would be of interest to examine what will be happen when different initial guess is considered. The computational conditions are the same as the previous case except that the initial guess is now chosen as $f(x,y,t)^0 = 0.06$ m.

Using stopping criterion $\varepsilon = 500$, after 22 iterations the inverse solutions for the estimated surface shapes at $t = 50$ and 150 s are shown in Fig. 6a and b, respectively. The relative average errors

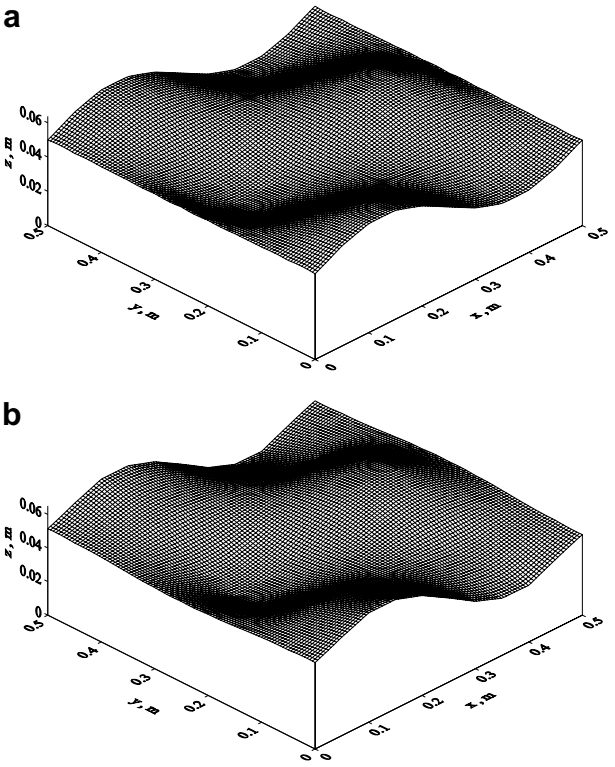

Fig. 2. The (a) exact and (b) estimated surface configurations $f(x,y,50)$ at $t = 50$ s with $\sigma = 0.0$ and $f(x,y,t)^0 = 0.04$ m in case 1.

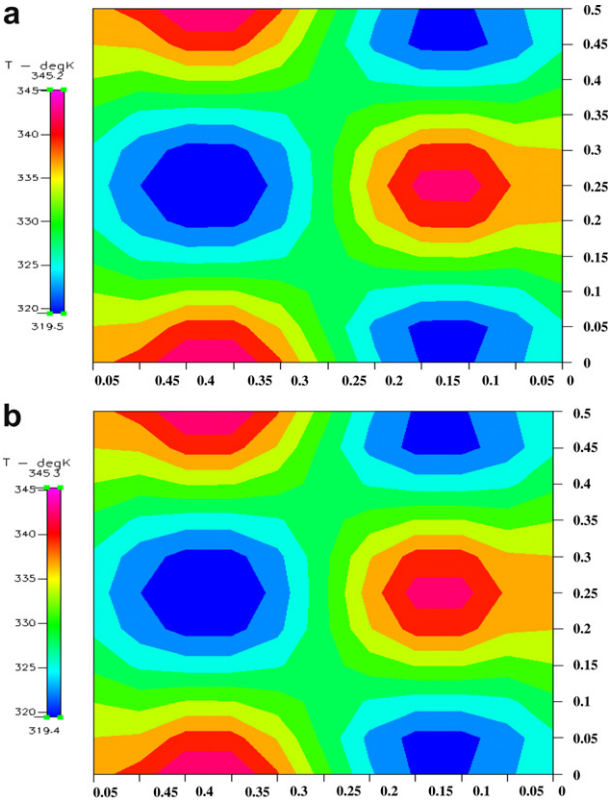

Fig. 3. The (a) measured and (b) estimated surface temperatures on S_{bottom} at $t = 50$ s with $\sigma = 0.0$ and $f(x,y,t)^0 = 0.04$ m in case 1.

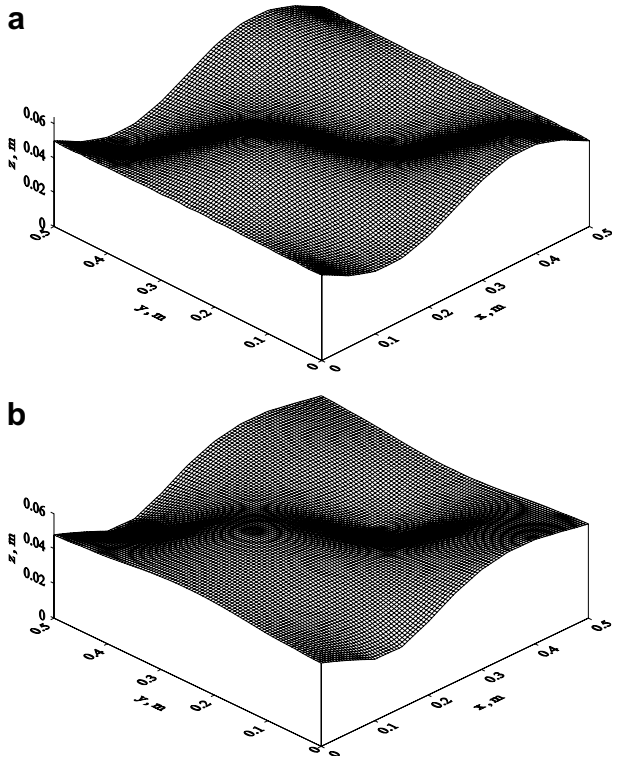

Fig. 4. The (a) exact and (b) estimated surface configurations $f(x,y,150)$ at $t = 150$ s with $\sigma = 0.0$ and $f(x,y,t)^0 = 0.04$ m in case 1.

ERR1 and ERR2 are calculated as ERR1 = 1.51% and ERR2 = 0.083%, respectively. The results are similar to those with $f(x,y,t)^0 = 0.04$ m. Therefore, it is clear from Fig. 6 and relative average errors that the estimated $f(x,y,t)$ is still very accurate when the initial guess for surface shapes is varied.

Finally, the influence of the measurement errors on the inverse solutions will be discussed. First, the measurement error for the simulated temperatures measured by infrared scanner on bottom surface S_{bottom} is taken as $\sigma = 0.62$ (about 1% of the average temperature measured on S_{bottom}). The estimations for $f(x,y,t)$ can be obtained after only 14 iterations and plotted in Fig. 7a and b for $t = 50$ and 150 s, respectively. The relative average errors ERR1 and ERR2 are calculated as ERR1 = 2.19% and ERR2 = 0.12%, respectively. The measurement error for the temperatures is then increased to $\sigma = 1.24$ (about 2% of the average temperature measured on S_{bottom}). After only eight iterations the estimated $f(x,y,t)$ are obtained and illustrated in Fig. 8a and b for $t = 50$ and 150 s, respectively. ERR1 and ERR2 are calculated as 3.22% and 0.24%, respectively. From those results it is learned that the reliable boundary configurations can still be obtained when large measurement errors are added.

9.2. Numerical test case 2

In the second test case, $f(x,y,t)$ is taken as

$$f(x,y,t) = \begin{cases} 0.05 + 0.001 \times y + 0.01 \times \sin\left(\frac{2\pi t}{200}\right) \times x; \\ \quad 0 \leqslant x \leqslant 0.15 \\ 0.05 + 0.001 \times y + 0.01 \times \sin\left(\frac{2\pi t}{200}\right) \times 3 - 0.015 \\ \quad \times \sin\left(\frac{2\pi t}{200}\right) \times (x-3); \quad 0.15 < x \leqslant 0.25 \\ 0.05 + 0.001 \times y + 0.015 \times \sin\left(\frac{2\pi t}{200}\right) \times (x-5); \\ \quad 0.25 < x \leqslant 0.4 \\ 0.05 + 0.001 \times y + 0.015 \times \sin\left(\frac{2\pi t}{200}\right) \times 3 - 0.02 \\ \quad \times \sin\left(\frac{2\pi t}{200}\right) \times (x-8); \quad 0.4 < x \leqslant 0.5 \end{cases} \tag{21}$$

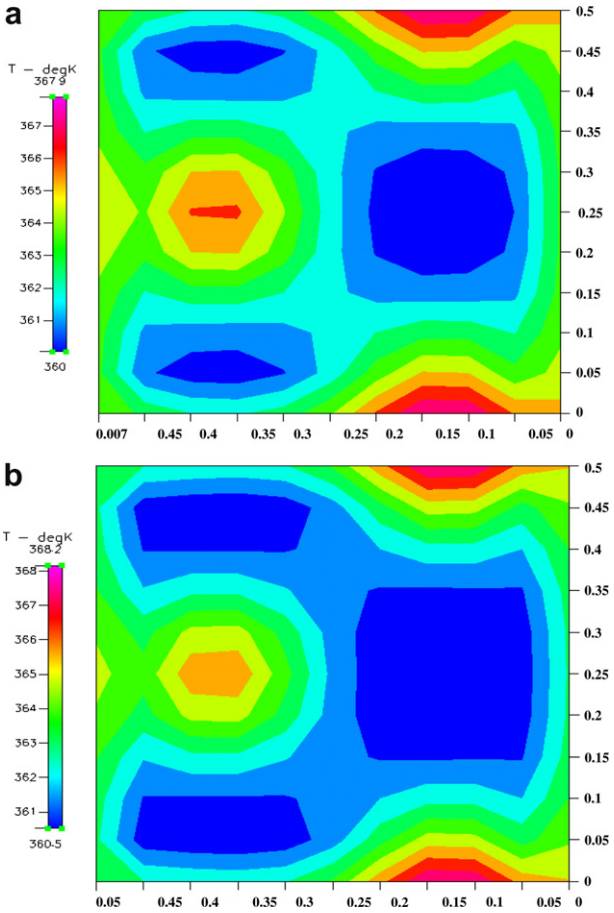

Fig. 5. The (a) measured and (b) estimated surface temperatures on S_{bottom} at $t = 150$ s with $\sigma = 0.0$ and $f(x,y,t)^0 = 0.04$ m in case 1.

The initial guess for this test case is chosen as $f(x,y)^0 = 0.04$ m. The inverse analysis is first performed by using $q = -50{,}000$ W/m^2 and assuming exact measurements, i.e. $\sigma = 0.0$ and using initial guess $f(x,y,t)^0 = 0.04$ m with convergent criterion $\varepsilon = 500$. The exact $f(x,y,t)$ in the above Eq. (21) at $t = 50$ s is shown in Fig. 9a. The estimated $f(x,y,t)$ can be obtained after 39 iterations and is plotted in Fig. 9b at $t = 50$ s. The measured and estimated surface temperatures on S_{bottom} are illustrated in Fig. 10a and b, respectively, at $t = 50$ s.

Similarly, the estimated results for boundary shapes and temperatures at $t = 150$ s are shown in Figs. 11 and 12, respectively. The average relative errors for the exact and estimated surface configurations and for the measured and estimated temperatures are calculated ERR1 = 2.21% and ERR2 = 0.071%, respectively.

Next, let us consider the influence of the measurement errors on the inverse solutions. First, the measurement error for the simulated temperatures measured by infrared scanner on bottom surface S_{bottom} is taken as $\sigma = 0.72$ (about 1% of the average temperature measured on S_{bottom}). After only 14 iterations, the estimations for $f(x,y,t)$ can be obtained and are plotted in Fig. 13a and b for $t = 50$ and 150 s, respectively. The relative average errors ERR1 and ERR2 are calculated as ERR1 = 3.46% and ERR2 = 0.14%, respectively.

The measurement error for the temperatures is then increased to $\sigma = 1.44$ (about 2% of the average temperature measured on S_{bottom}). After only eight iterations the estimated $f(x,y,t)$ are obtained and illustrated in Fig. 14a and b for $t = 50$ and 150 s, respectively. ERR1 and ERR2 are calculated as 5.15% and 0.29%, respectively.

From the above two numerical test cases, it is concluded that the advantages of the SDM in estimating unknown surface config-

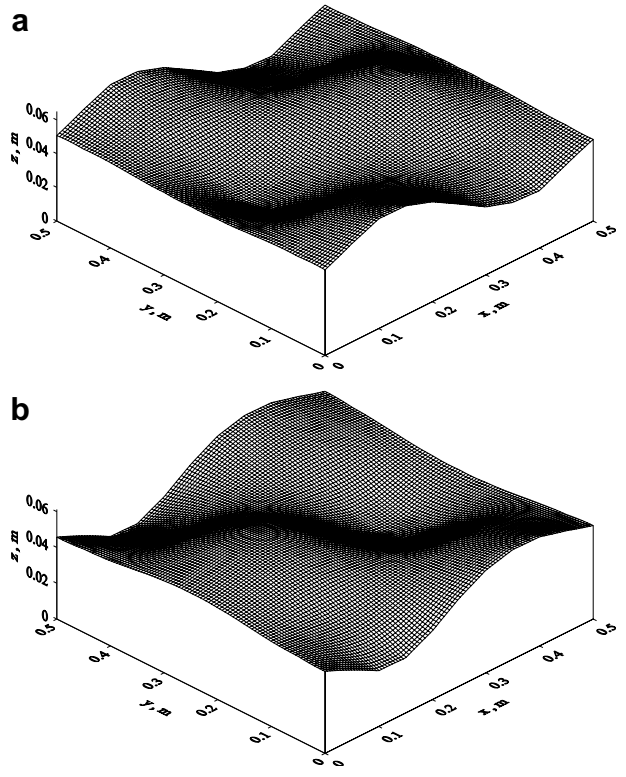

Fig. 6. The estimated surface configurations $f(x,y,t)$ with $\sigma = 0.0$ and $f(x,y,t)^0 = 0.06$ m in case 1 at (a) $t = 50$ s and (b) $t = 150$ s.

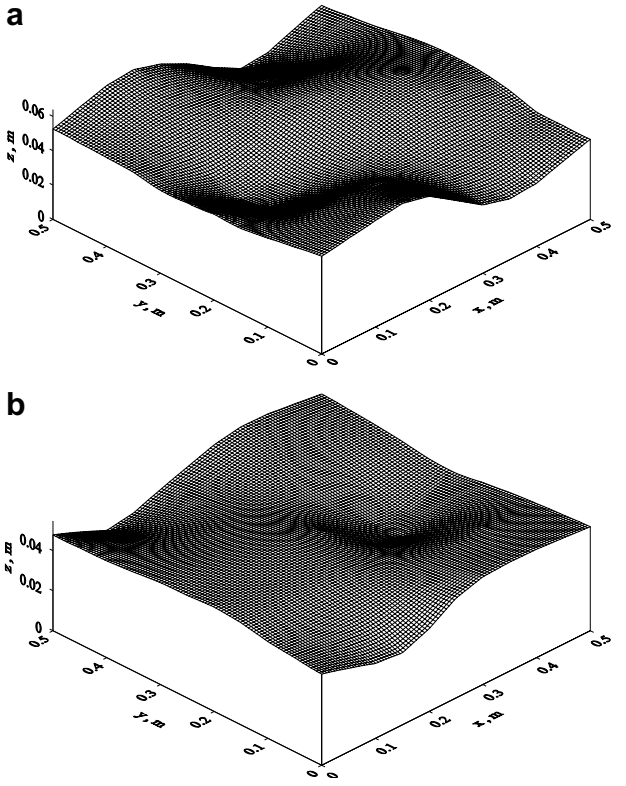

Fig. 8. The estimated surface configurations $f(x,y,t)$ with $\sigma = 1.24$ and $f(x,y,t)^0 = 0.04$ m in case 1 at (a) $t = 50$ s and (b) $t = 150$ s.

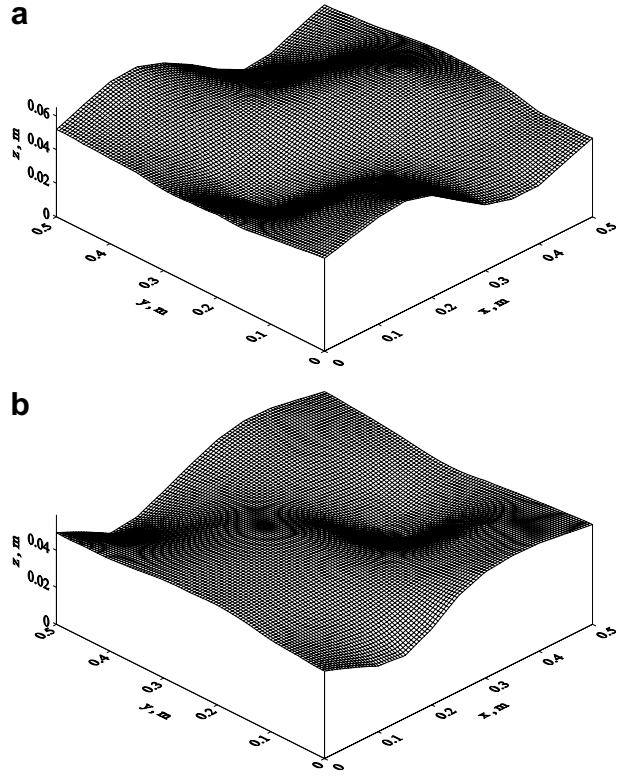

Fig. 7. The estimated surface configurations $f(x,y,t)$ with $\sigma = 0.62$ and $f(x,y,t)^0 = 0.04$ m in case 1 at (a) $t = 50$ s and (b) $t = 150$ s.

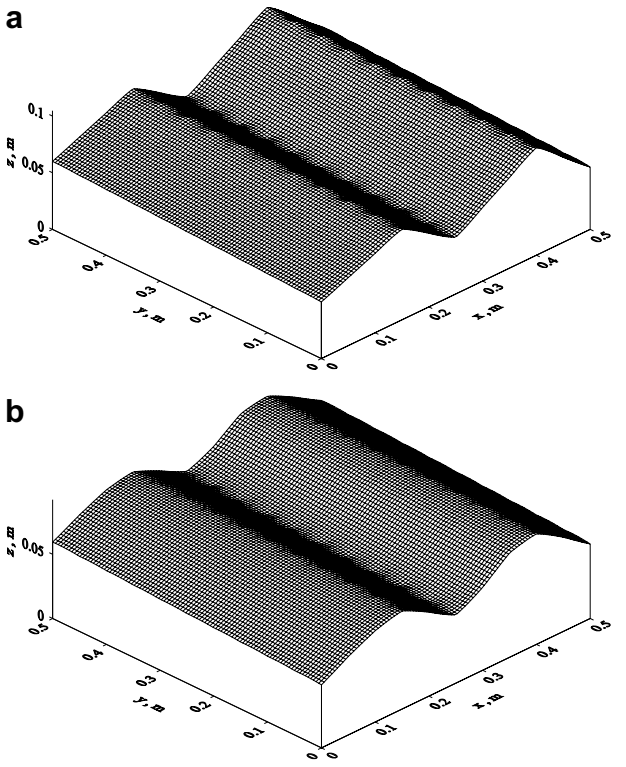

Fig. 9. The (a) exact and (b) estimated surface configurations $f(x,y,50)$ at $t = 50$ s with $\sigma = 0.0$ and $f(x,y,t)^0 = 0.04$ m in case 2.

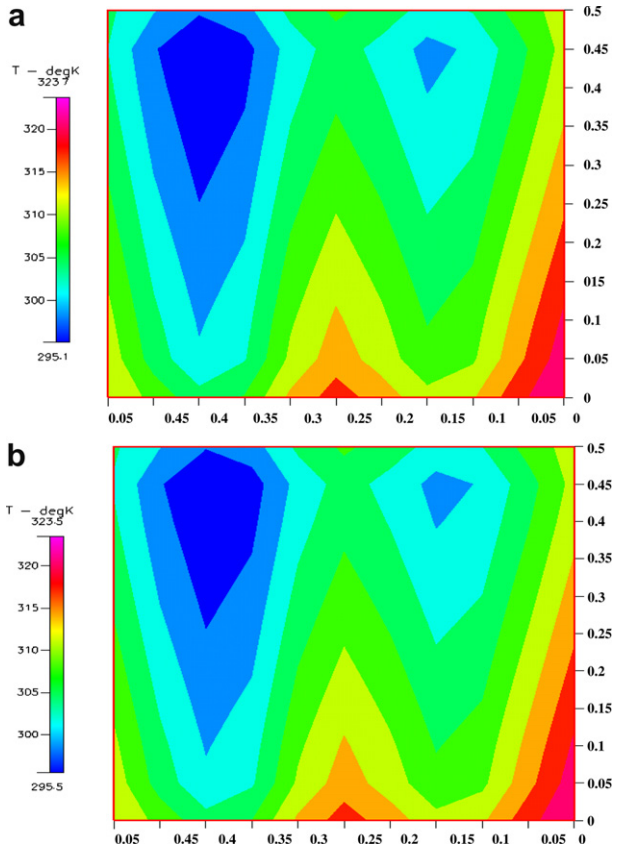

Fig. 10. The (a) measured and (b) estimated surface temperatures on S_{bottom} at $t = 50$ s with $\sigma = 0.0$ and $f(x,y,t)^0 = 0.04$ m in case 2.

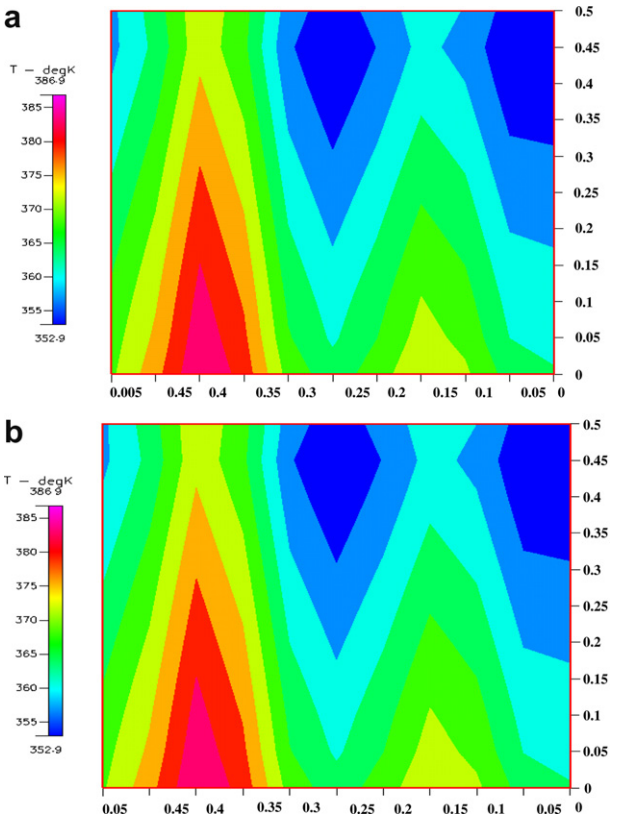

Fig. 12. The (a) measured and (b) estimated surface temperatures on S_{bottom} at $t = 150$ s with $\sigma = 0.0$ and $f(x,y,t)^0 = 0.04$ m in case 2.

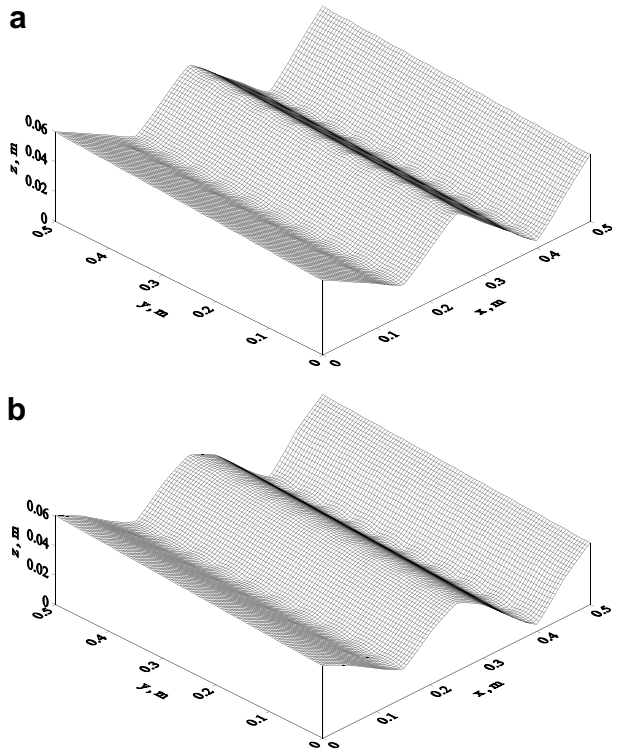

Fig. 11. The (a) exact and (b) estimated surface configurations $f(x,y,150)$ at $t = 150$ s with $\sigma = 0.0$ and $f(x,y,t)^0 = 0.04$ m in case 2.

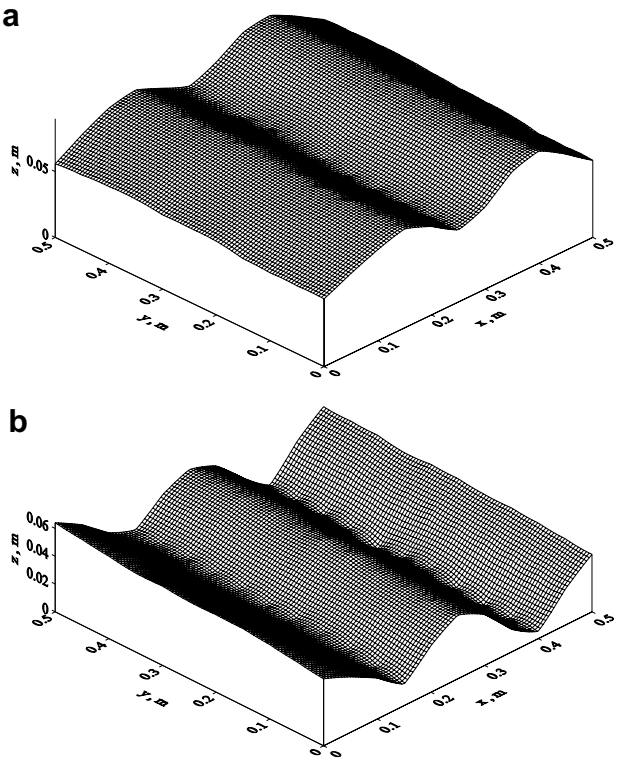

Fig. 13. The estimated surface configurations $f(x,y,t)$ with $\sigma = 0.72$ and $f(x,y,t)^0 = 0.04$ m in case 2 at (a) $t = 50$ s and (b) $t = 150$ s.

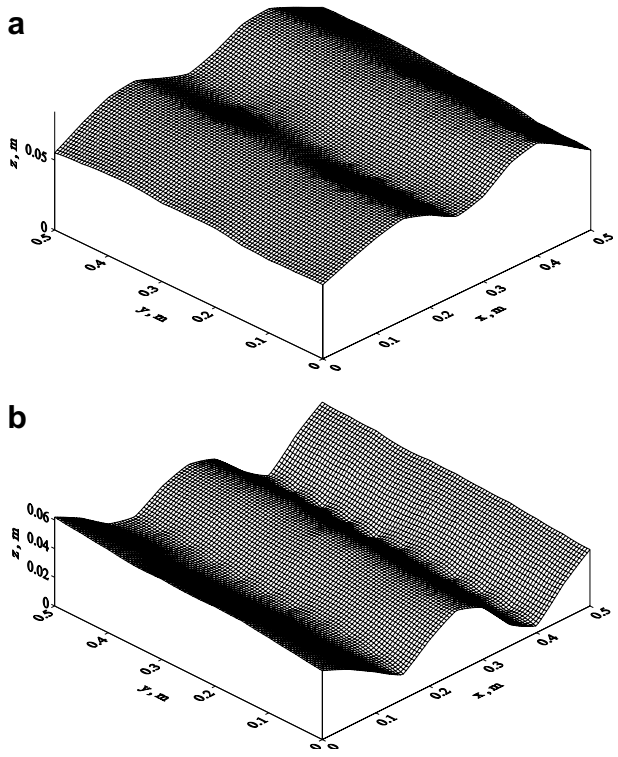

Fig. 14. The estimated surface configurations $f(x,y,t)$ with $\sigma = 1.44$ and $f(x,y,t)^0 = 0.04$ m in case 2 at (a) $t = 50$ s and (b) $t = 150$ s.

urations lie in that (i) it does not require a very accurate initial guess and (ii) the rate of convergence is fast.

10. Conclusions

The steepest descent method (SDM) and the commercial code CFD-RC are successfully applied for the solution of the three-dimensional transient inverse geometry problem in determining the unknown time and space-dependent irregular boundary configurations by utilizing simulated surface temperature measurements. Several test cases involving different initial guess, functional forms of $f(x,y,t)$ and measurement errors were considered. The results show that the SDM does not require an accurate initial guess of the unknown quantities and needs very few numbers of iterations in performing the inverse calculations on Pentium IV-30 GHz PC.

Acknowledgement

This work was supported in part through the National Science Council, ROC, Grant number, NSC-96-2221-E-006-065.

References

[1] C.H. Huang, W.C. Chen, A three-dimensional inverse forced convection problem in estimating surface heat flux by conjugate gradient method, Int. J. Heat Mass Transfer 43 (2000) 3171–3181.
[2] C.H. Huang, C.Y. Huang, An inverse biotechnology problem in estimating the optical diffusion and absorption coefficients of tissue, Int. J. Heat Mass Transfer 47 (2004) 447–457.
[3] C.H. Huang, H.C. Lo, A three-dimensional inverse problem in predicting the heat fluxes distribution in the cutting tools, Numer. Heat Transfer, Part A – Appl. 48 (2005) 1009–1034.
[4] A.J. Kassab, J. Pollard, A cubic spline anchored grid pattern algorithm for high resolution detection of subsurface cavities by the IR-CAT method, Numer. Heat Transfer, Part B 26 (1994) 63–78.
[5] G.S. Dulikravich, T.J. Martin, Inverse design of super-elliptic cooling passages in coated turbine blade airfoil, J. Thermophys. Heat Transfer 8 (1994) 288–294.
[6] K. Dems, Z. Mroz, Variational approach to sensitivity analysis in thermoelasticity, J. Therm. Stresses 10 (1987) 283–306.
[7] T. Burczynski, W. Beluch, A. Dlugosz, W. Kus, M. Nowakowski, P. Orantek, Evolutionary computation in optimization and identification, Comput. Assist. Mech. Eng. Sci. 9 (2002) 3–20.
[8] T. Burczinski, J.H. Kane, C. Balakrishna, Shape design sensitivity analysis via material derivative-adjoint variable technique for 3D and 2D curved boundary elements, Int. J. Numer. Methods Eng. 38 (1995) 2839–2866.
[9] C.H. Cheng, C.Y. Wu, An approach combining body-fitted grid generation and conjugate gradient methods for shape design in heat conduction problems, Numer. Heat Transfer B 37 (2000) 69–83.
[10] C.H. Huang, B.H. Chao, An inverse geometry problem in identifying irregular boundary configurations, Int. J. Heat Mass Transfer 40 (1997) 2045–2053.
[11] C.H. Huang, C.C. Tsai, A transient inverse two-dimensional geometry problem in estimating time-dependent irregular boundary configurations, Int. J. Heat Mass Transfer 41 (1998) 1707–1718.
[12] C.H. Huang, C.C. Chiang, H.M. Chen, Shape identification problem in estimating the geometry of multiple cavities, AIAA, J. Thermophys. Heat Transfer 12 (1998) 270–277.
[13] C.H. Huang, H.M. Chen, An inverse geometry problem of identifying growth of boundary shapes in a multiple region domain, Numer. Heat Transfer, Part A 35 (1999) 435–450.
[14] C.H. Huang, C.C. Shih, A shape identification problem in estimating simultaneously two interfacial configurations in a multiple region domain, Appl. Therm. Eng. 26 (2006) 77–88.
[15] E. Divo, A.J. Kassab, F. Rodriguez, An efficient singular superposition technique for cavity detection and shape optimization, Numer. Heat Transfer, Part B 46 (2004) 1–30.
[16] CFD-RC user's manual, ESI-CFD Inc., 2005.
[17] O.M. Alifanov, Inverse Heat Transfer Problems, Springer-Verlag, Berlin Heidelberg, 1994.
[18] IMSL Library Edition 10.0, User's Manual: Math Library Version 1.0, IMSL, Houston, TX, 1987.